DNA Nanoimprinting

Deutsche Ausgabe: DOI: 10.1002/ange.201512022
Internationale Ausgabe: DOI: 10.1002/anie.201512022

Transfer of Two-Dimensional Oligonucleotide Patterns onto Stereocontrolled Plasmonic Nanostructures through DNA-Origami-Based Nanoimprinting Lithography

Yinan Zhang[+], Jie Chao[+], Huajie Liu, Fei Wang, Shao Su, Bing Liu, Lan Zhang, Jiye Shi, Lihua Wang, Wei Huang, Lianhui Wang,* and Chunhai Fan**

Abstract: *The precise functionalization of self-assembled nanostructures with spatial and stereocontrol is a major objective of nanotechnology and holds great promise for many applications. Herein, the nanoscale addressability of DNA origami was exploited to develop a precise copy-machine-like platform that can transfer two-dimensional oligonucleotide patterns onto the surface of gold nanoparticles (AuNPs) through a deliberately designed toehold-initiated DNA displacement reaction. This strategy of DNA-origami-based nanoimprinting lithography (DONIL) demonstrates high precision in controlling the valence and valence angles of AuNPs. These DNA-decorated AuNPs act as precursors in the construction of discrete AuNP clusters with desired chirality.*

Self-assembled nanostructures have shown great potential in nanoelectronics,[1] nanophotonics,[2] and biomedicines[3] as a result of their tailorable optical/electronic properties and unique chemical/biological activities.[4] Although there has been remarkable progress in the synthesis of nanoparticles (NPs) with controlled size, shape, and composition,[5] the goal of precise functionalization of NPs for the creation of molecule-like discrete nanostructures with customized shape and design is yet to be achieved. As a result of its ability to recognize nonparallel base-pairing, DNA can be used as part of a highly flexible programmable route for the construction of nanostructures, and it has recently received increased attention for this purpose.[6] For example, DNA has been exploited in the functionalization of various types of nanomaterials, including metals (for example, Au, Ag),[7] semiconductors (such as, quantum dots and polymer dots),[8] insulators (for example, upconversion and metal oxides), NPs,[9] and a range of carbon nanomaterials.[1a,10]

DNA-functionalized gold NPs (DNA-AuNPs) are among the most studied nanobiological systems.[11] Efforts have been made to control the density and orientation of DNA strands on AuNPs,[12] which have proven useful in a wide range of applications, including diagnosis, drug delivery, bioimaging, catalysis, and metamaterials.[13] More recently, several groups have developed new strategies for regulated anchoring of DNA on AuNPs using either steric control or nanocage encapsulation to make "atom-like" AuNPs with a fixed number of DNA strands.[14] However, whereas nearly perfect valence control has been realized, bond anisotropy is often poorly defined in these procedures. Very recently, Sleiman et al. proposed a strategy in which DNA patterns were transferred from DNA framework nanostructures onto 10 nm AuNPs.[15]

DNA origami is a rapidly emerging technology providing unprecedented power in precise organization.[16] In a typical DNA origami assembly process, about 200 short, designed sequences serve as "staples" to fold a long, single-stranded DNA (ssDNA) scaffold into virtually any prescribed shape or pattern. Each staple strand acts as a recognition site for anchoring molecules or nanomaterials with excellent addressability.[17] Many successful applications have taken advantage of the organizational power of DNA origami, including the organization of CpG oligonucleotides and siRNAs for therapeutic uses,[18] enzyme pairs for artificial cascades,[19] conjugated polymers[20] and carbon nanotubes[1a] for nanoelectronics, and AuNPs for plasmonic applications.[21] However, these types of organization rely on static, prescribed DNA origami designs, whereas dynamic systems have been little exploited.[22] In this study, we developed a DNA-origami-based nanoimprinting lithography (DONIL) strategy for stereocontrolled assembly of DNA-AuNPs with a fixed number of DNA strands (valence) and anisotropy (bond angle and DNA sequence specificity). By deliberately placing DNA "set strands" with predefined numbers, sequences, and positions on an origami structure, we demonstrated that such two-dimensional information could be transferred on the

[*] Y. Zhang,[+] Prof. J. Chao,[+] Prof. S. Su, Prof. W. Huang, Prof. L. Wang
Key Laboratory for Organic Electronics & Information Displays (KLOEID), Institute of Advanced Materials (IAM) and School of Materials Science and Engineering
Nanjing University of Posts & Telecommunications Institution
9 Wenyuan Road, Nanjing 210046 (China)
E-mail: iamlhwang@njupt.edu.cn

Y. Zhang,[+] Prof. H. Liu, F. Wang, B. Liu, Prof. L. Zhang, Prof. L. Wang, Prof. C. Fan
Division of Physical Biology and Bioimaging Center
Shanghai Synchrotron Radiation Facility
CAS Key Laboratory of Interfacial Physics and Technology
Shanghai Institute of Applied Physics
Chinese Academy of Sciences, Shanghai 201800 (China)
E-mail: liuhuajie@sinap.ac.cn
fchh@sinap.ac.cn

Dr. J. Shi
Kellogg College, University of Oxford
Oxford, OX2 6PN (UK)

Dr. J. Shi
UCB Pharma
208 Bath Road, Slough, SL1 3WE (UK)

[+] These authors contributed equally to this work.

Supporting information for this article can be found under: http://dx.doi.org/10.1002/anie.201512022.

surface of AuNPs, reminiscent of the function of a copy machine. Thus, prepared DNA-AuNPs exhibited fixed valence, orientation, and bonding anisotropy, forming the basis for the construction of discrete, chiral plasmonic nanostructures with controlled geometry, composition, and isomerism.

Figure 1 schematically depicts the working principle of our DNA origami transfer method functioning by means of DONIL. In this method, citrate-stabilized AuNPs of diameter 30 nm are first densely coated with a 30 nucleotide (30 nt) thiolated sequence (coat strand). On the DNA origami scaffold, staple strands at prescribed sites act as sequence-specific set-hold strands that can fix their corresponding set strands. A T_3 spacer is used in each set-hold strand to connect the set-hold domain to the staple domain. Here, three

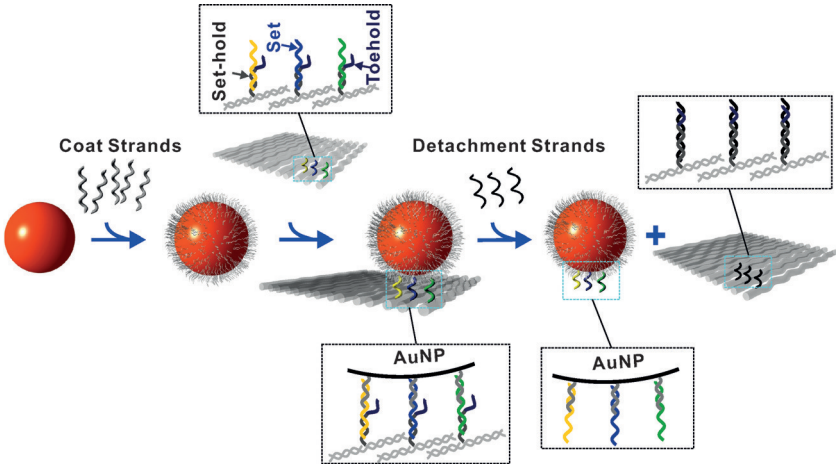

Figure 1. Working principle of the DNA origami transfer method which operates through DNA-origami-based nanoimprinting lithography (DONIL).

different set and set-hold strands pairs are positioned in a linear array with a defined spacing, with each set strand consisting of two domains: the anti-hold domain, which is complementary to a set-hold strand, and the anti-coat domain, which can bind to the coat strand on AuNPs. An 8 nt toehold domain is reserved in each set-hold strand for the subsequent strand displacement reactions.[23] For loading, AuNPs are incubated with the DNA origami template and set strands are used to help anchor them onto the defined sites. In this case, a 30 nm AuNP is loaded onto the DNA origami in a 1:1 manner through three set and coat strand pairs, which sterically hinders the loading of another AuNP. Then, detachment strands are introduced, which are fully complementary to set-hold strands. They nucleate at toehold domains to initiate strand migrations and finally detach the set strands from the DNA origami. As a result, the AuNP is released while the set strand patterns are precisely transferred onto its surface. Since the number, positions, and sequences of set strands are predefined, the DNA on the AuNP is expected to have defined valence, site specificity, and sequence anisotropy.

To demonstrate the feasibility of this approach, we first attempted to prepare a trivalent DNA-AuNP conjugate with three DNA modifications arranged according to C_{2v} symmetry (Figure 2a) by DONIL. One set A and two set B strands were positioned in a linear array (in B-A-B order) on a rectangular DNA origami template. AuNPs were then mixed with the DNA origami template, and AuNP–DNA origami conjugates were purified with agarose gel electrophoresis (see Figure S1a in the Supporting Information). According to atomic force microscopy (AFM) measurements, the loading yield of the 1:1 AuNP–DNA origami conjugates was greater than 85% (Table S2). The trivalent DNA-AuNP products were then obtained after the detachment of the set strands from DNA origami templates. Waste DNA strands were removed through centrifugation. Gel electrophoresis and AFM characterization confirmed the success of this procedure (Figure S2).

The trivalent product contains two components: monovalent set A and divalent set B strands, which are spatially resolved. To validate the quality of the prepared AuNPs, we selectively constructed several high-order, discrete structures to demonstrate their features. First, we designed a "bridge duplex" to join two DNA-AuNPs into a homodimer (Figure 2b). To this end, one bridge or anti-bridge strand was attached to a trivalent DNA-AuNP using the monovalent set A strand, forming two complementary AuNPs. Agarose gel electrophoresis indicated that a new band had appeared in the mixture of these two AuNPs, with no other heavy aggregates found. The homodimer morphology of the product extracted from the gel was confirmed with transmission electron microscopy (TEM) imaging. In another demonstration, trivalent AuNPs were incubated with excess 20 nm AuNPs with the intention of obtaining a heterodimeric product (Figure 2c). The 20 nm AuNPs were densely packed with a thiolated DNA sequence complementary to the set A strand. Agarose gel and TEM characterization again demonstrated that only heterodimeric product was formed. Noticeably, although an excess of 20 nm AuNPs were used, they hybridized with 30 nm trivalent AuNPs in a strict 1:1 manner, and no crosstalk occurred. These results confirm that the set A modification is monovalent. The yields of the homo- and heterodimer products were estimated at 30% and 43%, respectively (Table S3). We also used 10 nm and 15 nm AuNPs to build heterodimers (Figures 2d,e; Figures S3, S4). Similarly, to confirm the divalent nature of set B strands, a heterotrimeric structure was successfully constructed through the assembly of one trivalent AuNP with two small AuNPs (5 nm) capable of recognizing set B strands (Figure 2f). Trimer yields were calculated to be 63% (Table S3).

Three-component trivalent decoration of AuNPs can also be produced through DONIL. As shown in Figure 2g (also in Figures S5, S6), three different set strands (set A, B, and C) are positioned linearly. As a result of the sequence inhomogeneity, the real symmetry of this linear pattern on AuNPs

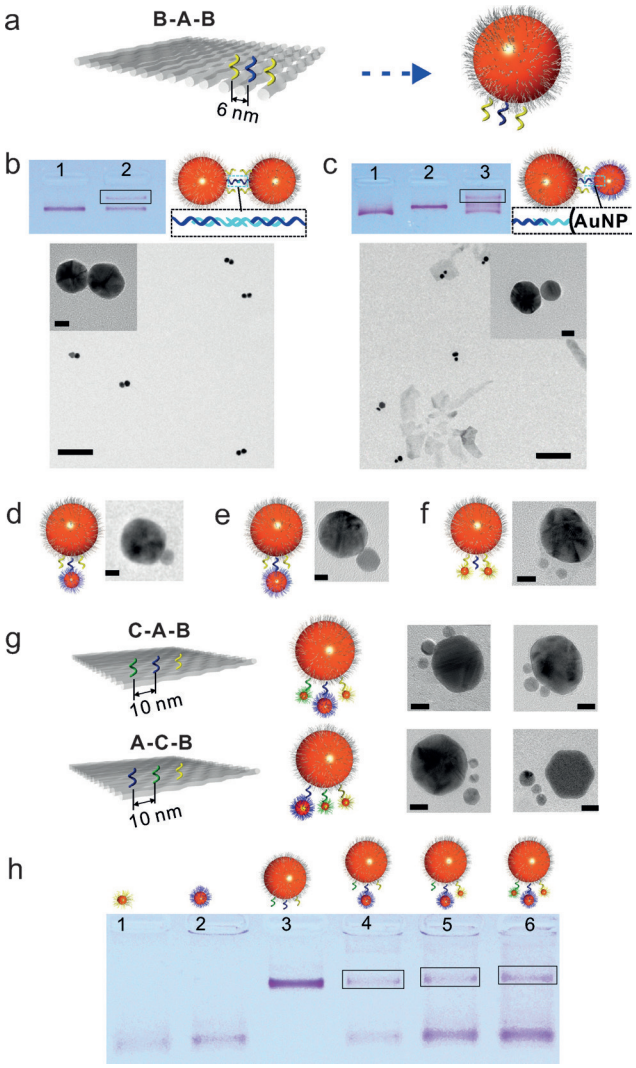

Figure 2. The transfer of trivalent, multicomponent DNA to form linearly decorated AuNPs and discrete AuNP clusters. a) Transfer of a linear array (B-A-B order) from DNA origami to an AuNP (30 nm) surface. b) Agarose gel and TEM analysis of homodimers formed by two B-A-B trivalent DNA-AuNPs. Lane 1: trivalent DNA-AuNPs; lane 2: trivalent DNA-AuNPs + bridge duplexes. c) Agarose gel and TEM analysis of heterodimers formed by trivalent DNA-AuNPs (30 nm) with densely packed DNA-AuNPs (20 nm). Lane 1: 20 nm densely packed DNA-AuNPs; lane 2: trivalent DNA-AuNPs; lane 3: mixture of two kinds of DNA-AuNPs. TEM scale bars in (b, c) = 200 nm (insets = 10 nm). d–f) Other discrete AuNP clusters: 30 nm/10 nm heterodimer (d), 30 nm/15 nm heterodimer (e), 30 nm/5 nm/5 nm trimer (f). g) Tetramers formed by trivalent DNA-AuNPs (30 nm) with three kinds of small, densely packed DNA-AuNPs arranged in C-A-B and A-C-B orders. Scale bars in (d–g) = 10 nm. h) Agarose gel analysis of tetramers formed by C-A-B trivalent DNA-AuNPs. Lanes: 1) 5 nm DNA-AuNPs; 2) 10 nm DNA-AuNPs; 3) trivalent DNA-AuNPs; 4) trivalent DNA-AuNPs + 10 nm DNA-AuNPs; 5) trivalent DNA-AuNPs + 10 nm DNA-AuNPs + 5 nm DNA-AuNPs; 6) trivalent DNA-AuNPs + 10 nm DNA-AuNPs + two types of 5 nm DNA-AuNPs. In all cases, the starting trivalent DNA-AuNP has a diameter of 30 nm.

reduces to C_s, but not C_{2v}. Importantly, the arrangement of these three set strands can be adjusted by simply changing their positions. To verify this feature, three small AuNPs (10 nm and 5 nm) with different complementarities were assembled on an as-prepared 30 nm trivalent AuNP in either C-A-B or A-C-B order. Low mobility bands were observed on agarose gels, indicating the formation of large AuNP clusters (Figure 2h). TEM images further confirmed that both products were monodispersed tetramers but with different conformations. In the C-A-B ordered sample, one 10 nm AuNP stands in the middle of two 5 nm AuNPs. In contrast, two 5 nm AuNPs are placed together in the A-C-B ordered sample.

We next demonstrated that this method could be extended to multivalent AuNPs with controllable valence angles. In a typical design, four set strands are located at the four corners of a rectangle on a DNA origami template (Figure 3a). According to the nano-addressability desired, the distance between these set strands could be adjusted, altering the valence angle on the AuNPs since positional information is transferred from the flat origami to the curved AuNP. The valence angle, θ, in the triangle COD (Figure 3b), can be theoretically calculated from Equation (1) under ideal

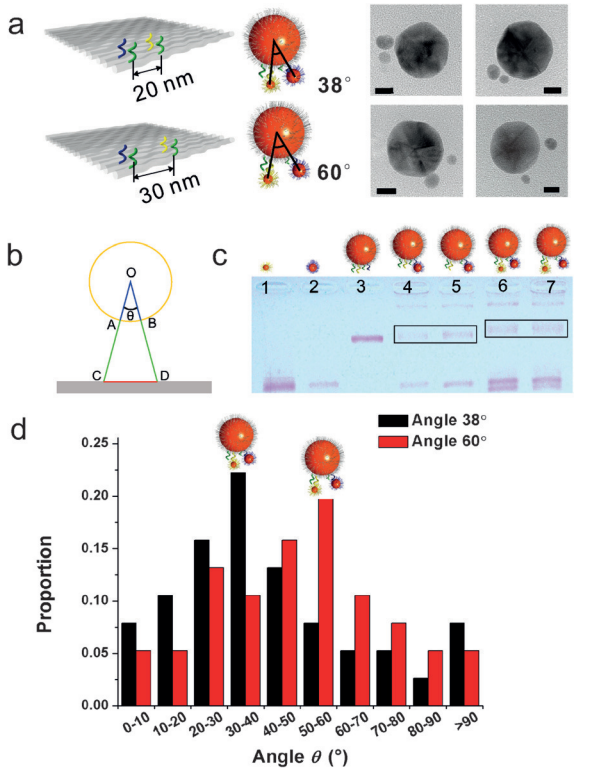

Figure 3. Regulation of the valence angle on AuNPs. a) Regulation of the valence angle by alteration of the distance between DNA strands. b) Calculation of the valence angle on valence-controlled AuNPs. Distance OA depends on the radius of the AuNP, and AC is the length of the duplex, which can be calculated as $0.34 \times n$ (where n denotes the number of base pairs). Length CD can be adjusted by varying the position of set-hold strands. c) Agarose gel analysis of AuNPs with controllable valence angles, using a 30 nm DNA-AuNP as the central unit at point O. Lanes: 1) 5 nm densely packed DNA-AuNPs; 2) 10 nm densely packed DNA-AuNPs; 3) 38° DNA-AuNPs; 4) 38° DNA-AuNPs + 10 nm DNA-AuNPs; 5) 60° DNA-AuNPs + 10 nm DNA-AuNPs; 6) 38° DNA-AuNPs + 10 nm DNA-AuNPs + 5 nm DNA-AuNPs; 7) 60° DNA-AuNPs + 10 nm AuNPs + 5 nm AuNPs. d) Distribution of the resulting valence angles in different designs.

conditions (where, for example, OC is the length of the "triangle" between apices O and C):

$$\cos\theta = \frac{OC^2 + OD^2 - CD^2}{2OC \times OD} \quad (1)$$

As a simple example, we constructed a three-component pattern, with set A and set B strands located at two corners and set C strands anchored on the other two corners. The positions of the set A and set B strands can be adjusted to achieve angle control in the subsequent steps, while the set C strands are used to aid in the loading of AuNPs onto the DNA origami platform. Calculations revealed that each 5 nm increase in the distance between set A and set B will lead to an 11° enlargement in their valence angle on a 30 nm AuNP (Figure 3b). We first attempted a small distance of 20 nm, which corresponds to a 38° valence angle on an AuNP. By increasing the distance to 30 nm, it is expected that the valence angle would be enlarged to 60°. After transfer of positional information through the aforementioned procedure, 10 nm and 5 nm AuNPs complementary to set A and set B strands, respectively, were used for quality assurance. As shown in Figure 3c, a new band with low mobility appeared on the agarose gel after incubating tetravalent DNA-AuNPs with their complementary, small AuNPs. TEM characterization confirmed that these represent heterotrimers, as expected. It is worth noting that based on gel results, trimers with different valence angles cannot be differentiated. However, valence angles can be approximated by counts from TEM images (Figures S7–9), though dehydration of prepared samples may lead to deformation to some degree. The analysis presented in Figure 3d reveals that the distribution of valence angles matches our design.

We were then motivated to further explore the possibility of using this strategy to obtain multicomponent patterns on AuNPs with controlled stereoisomerism. To achieve this goal, DNA modifications on AuNPs must be far enough apart to avoid random disturbances and steric bulk effects. Unfortunately, it is considerably more difficult to transfer a large pattern from a flat DNA origami surface to a curved AuNP. Therefore, a triangular DNA origami template with a cavity in the center was utilized to allow the stable assembly of 30 nm AuNPs and effective transfer of pattern information. This in turn creates a larger range of valences and valence angles. In this way, we produced trivalent DNA-AuNPs decorated with up to three components with 30 nm spacing (Figure 4a). The apparent symmetry of this pattern is C_{3v}, but when considering the sequence specificity, the real symmetry can be reduced to C_1 (asymmetric). Hence, three different arrangements with specific chiralities were tested. The A-A-A arrangement has a typical C_{3v} symmetry, but the A-B-C and B-A-C arrangements are stereoisomers with only C_1 symmetry. Accordingly, three AuNPs of different sizes (10 nm, 15 nm, and 20 nm) were involved in the assembly of the trivalent AuNPs. In addition to TEM characterization (Figure 4b), circular dichroism (CD) spectroscopy measurements were carried out to ascertain the chiralities (Figure S10). Although the absorption spectra of the arrangements (Figure S11) are the same, they exhibit completely different CD behaviors. For the A-A-A arrangement, one 30 nm AuNP is linked with three 15 nm AuNPs, exhibiting no chirality at all. Noticeably, heterotetramers with A-B-C and B-A-C arrangements exhibit inverse CD characteristics, reflecting their chiral nature and further implying that they are enantiomers with opposite chiralities. These observations again confirm our design.

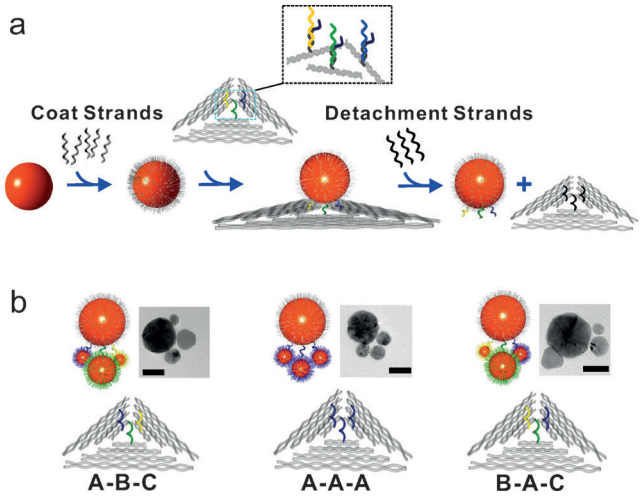

Figure 4. Stereocontrolled patterns for making chiral Au nanostructures. a) Schematic illustration of the transfer of a triangular pattern from a triangular DNA origami to an AuNP surface. b) Tetramers formed by trivalent stereospecific DNA-AuNPs with three kinds of small, densely packed DNA-AuNPs arranged in A-B-C, A-A-A, and B-A-C orders. TEM scale bars = 20 nm.

In summary, we have developed a conceptually new DONIL strategy to realize customized DNA patterning on AuNPs. Precise, DNA-origami-based copy-machine-like platforms possess the competitive advantage of perfect nano-addressability over competing approaches. Toehold-mediated strand displacement reactions aid in the precise transfer of positional information from DNA origami templates to curved AuNPs in a quantitative, directional, and sequence-specific manner. These prepared DNA-AuNPs are promising candidates for guiding the assembly of discrete AuNP clusters with control over valence, geometry, and symmetry. This method is also applicable to a system using multi-handle strands at one specific position, which will strengthen the binding between AuNPs. Looking further ahead, we envision that this DONIL strategy could be extended to more complex 3D patterns using the versatile DNA origami technology. Providing efficient shape matching between a DNA origami template and AuNPs, enlarged interfaces should allow arbitrary attachment of DNA tags to any position on a single AuNP. In addition, this mechanized platform is, in principle, applicable to other types of DNA-modified nano-objects, regardless of their shape or composition. Thus, we expect that this DONIL will be a generic strategy for the construction of novel nanostructures for catalysis, biosensors, imaging, and plasmonics.[13b,24]

Acknowledgements

This work was financially supported by the National Basic Research Program of China (973 Program, 2013CB932800, 2012CB932600, and 2013CB933802) and the National Natural Science Foundation of China (21473236, 31371015, 21227804, 21329501, and 21390414).

Keywords: DNA nanotechnology · gold · nanoimprinting lithography · nanoparticles · self-assembly

How to cite: *Angew. Chem. Int. Ed.* **2016**, *55*, 8036–8040
Angew. Chem. **2016**, *128*, 8168–8172

[1] a) H. T. Maune, S. P. Han, R. D. Barish, M. Bockrath, W. A. Iii, P. W. Rothemund, E. Winfree, *Nat. Nanotechnol.* **2010**, *5*, 61–66; b) K. Keren, R. S. Berman, E. Buchstab, U. Sivan, E. Braun, *Science* **2003**, *302*, 1380–1382.

[2] A. Kuzyk, R. Schreiber, Z. Fan, G. Pardatscher, E. M. Roller, A. Hogele, F. C. Simmel, A. O. Govorov, T. Liedl, *Nature* **2012**, *483*, 311–314.

[3] P. K. Lo, P. Karam, F. A. Aldaye, C. K. McLaughlin, G. D. Hamblin, G. Cosa, H. F. Sleiman, *Nat. Chem.* **2010**, *2*, 319–328.

[4] a) K. Manthiram, Y. Surendranath, A. P. Alivisatos, *J. Am. Chem. Soc.* **2014**, *136*, 7237–7240; b) E. C. Dreaden, A. M. Alkilany, X. Huang, C. J. Murphy, M. A. El-Sayed, *Chem. Soc. Rev.* **2012**, *41*, 2740–2779; c) Y. Zhou, Q. Huang, J. Gao, J. Lu, X. Shen, C. Fan, *Nucleic Acids Res.* **2010**, *38*, e156.

[5] A. M. Alkilany, S. E. Lohse, C. J. Murphy, *Acc. Chem. Res.* **2013**, *46*, 650–661.

[6] Z. Yang, H. Liu, D. Liu, *NPG Asia Mater.* **2015**, *7*, e161.

[7] a) A. P. Alivisatos, K. P. Johnsson, X. Peng, T. E. Wilson, C. J. Loweth, M. P. Bruchez, Jr., P. G. Schultz, *Nature* **1996**, *382*, 609–611; b) C. A. Mirkin, R. L. Letsinger, R. C. Mucic, J. J. Storhoff, *Nature* **1996**, *382*, 607–609; c) S. Pal, J. Sharma, H. Yan, Y. Liu, *Chem. Commun.* **2009**, 6059–6061.

[8] a) Z. Deng, A. Samanta, J. Nangreave, H. Yan, Y. Liu, *J. Am. Chem. Soc.* **2012**, *134*, 17424–17427; b) B. Datta, G. B. Schuster, A. McCook, S. C. Harvey, K. Zakrzewska, *J. Am. Chem. Soc.* **2006**, *128*, 14428–14429.

[9] a) L. L. Li, Y. Lu, *J. Am. Chem. Soc.* **2015**, *137*, 5272–5275; b) D. Nyamjav, A. Ivanisevic, *Biomaterials* **2005**, *26*, 2749–2757.

[10] a) L. Tang, Y. Wang, J. Li, *Chem. Soc. Rev.* **2015**, *44*, 6954–6980; b) H. Pei, J. Li, M. Lv, J. Wang, J. Gao, J. Lu, Y. Li, Q. Huang, J. Hu, C. Fan, *J. Am. Chem. Soc.* **2012**, *134*, 13843–13849.

[11] J. I. Cutler, E. Auyeung, C. A. Mirkin, *J. Am. Chem. Soc.* **2012**, *134*, 1376–1391.

[12] a) S. J. Hurst, A. K. Lytton-Jean, C. A. Mirkin, *Anal. Chem.* **2006**, *78*, 8313–8318; b) H. Pei, F. Li, Y. Wan, M. Wei, H. Liu, Y. Su, N. Chen, Q. Huang, C. Fan, *J. Am. Chem. Soc.* **2012**, *134*, 11876–11879; c) D. Zanchet, C. M. Micheel, W. J. Parak, D. Gerion, A. P. Alivisatos, *Nano Lett.* **2001**, *1*, 32–35; d) K. Suzuki, K. Hosokawa, M. Maeda, *J. Am. Chem. Soc.* **2009**, *131*, 7518–7519; e) Z. Li, E. Cheng, W. Huang, T. Zhang, Z. Yang, D. Liu, Z. Tang, *J. Am. Chem. Soc.* **2011**, *133*, 15284–15287; f) X. Zhang, M. R. Servos, J. Liu, *J. Am. Chem. Soc.* **2012**, *134*, 7266–7269; g) G. B. Yao, H. Pei, J. Li, Y. Zhao, D. Zhu, Y. N. Zhang, Y. F. Lin, Q. Huang, C. H. Fan, *NPG Asia Mater.* **2015**, *7*, e159.

[13] a) J. Zheng, G. Zhu, Y. Li, C. Li, M. You, T. Chen, E. Song, R. Yang, W. Tan, *ACS Nano* **2013**, *7*, 6545–6554; b) K. Li, K. Wang, W. Qin, S. Deng, D. Li, J. Shi, Q. Huang, C. Fan, *J. Am. Chem. Soc.* **2015**, *137*, 4292–4295; c) P. Chen, D. Pan, C. Fan, J. Chen, K. Huang, D. Wang, H. Zhang, Y. Li, G. Feng, P. Liang, L. He, Y. Shi, *Nat. Nanotechnol.* **2011**, *6*, 639–644; d) E. Boisselier, D. Astruc, *Chem. Soc. Rev.* **2009**, *38*, 1759–1782; e) W. Yan, L. Xu, C. Xu, W. Ma, H. Kuang, L. Wang, N. A. Kotov, *J. Am. Chem. Soc.* **2012**, *134*, 15114–15121; f) S. Shimron, A. Cecconello, C. H. Lu, I. Willner, *Nano Lett.* **2013**, *13*, 3791–3795.

[14] a) L. H. Tan, H. Xing, H. Chen, Y. Lu, *J. Am. Chem. Soc.* **2013**, *135*, 17675–17678; b) Y. Li, Z. Liu, G. Yu, W. Jiang, C. Mao, *J. Am. Chem. Soc.* **2015**, *137*, 4320–4323; c) Z. Zhao, E. L. Jacovetty, Y. Liu, H. Yan, *Angew. Chem. Int. Ed.* **2011**, *50*, 2041–2044; *Angew. Chem.* **2011**, *123*, 2089–2092.

[15] T. G. Edwardson, K. L. Lau, D. Bousmail, C. J. Serpell, H. F. Sleiman, *Nat. Chem.* **2016**, *8*, 162–170.

[16] a) P. W. Rothemund, *Nature* **2006**, *440*, 297–302; b) S. M. Douglas, H. Dietz, T. Liedl, B. Högberg, F. Graf, W. M. Shih, *Nature* **2009**, *459*, 414–418.

[17] a) B. Ding, Z. Deng, H. Yan, S. Cabrini, R. N. Zuckermann, J. Bokor, *J. Am. Chem. Soc.* **2010**, *132*, 3248–3249; b) B. Saccà, R. Meyer, M. Erkelenz, K. Kiko, A. Arndt, H. Schroeder, K. S. Rabe, C. M. Niemeyer, *Angew. Chem. Int. Ed.* **2010**, *49*, 9378–9383; *Angew. Chem.* **2010**, *122*, 9568–9573; c) S. S. Jia, J. Chao, C. H. Fan, H. J. Liu, *Prog. Chem.* **2014**, *26*, 695–705.

[18] V. J. Schüller, S. Heidegger, N. Sandholzer, P. C. Nickels, N. A. Suhartha, S. Endres, C. Bourquin, T. Liedl, *ACS Nano* **2011**, *5*, 9696–9702.

[19] J. Fu, M. Liu, Y. Liu, N. W. Woodbury, H. Yan, *J. Am. Chem. Soc.* **2012**, *134*, 5516–5519.

[20] J. B. Knudsen, L. Liu, A. L. Bank Kodal, M. Madsen, Q. Li, J. Song, J. B. Woehrstein, S. F. Wickham, M. T. Strauss, F. Schueder, J. Vinther, A. Krissanaprasit, D. Gudnason, A. A. Smith, R. Ogaki, A. N. Zelikin, F. Besenbacher, V. Birkedal, P. Yin, W. M. Shih, R. Jungmann, M. Dong, K. V. Gothelf, *Nat. Nanotechnol.* **2015**, *10*, 892–898.

[21] G. P. Acuna, F. M. Moller, P. Holzmeister, S. Beater, B. Lalkens, P. Tinnefeld, *Science* **2012**, *338*, 506–510.

[22] a) A. Kuzuya, Y. Ohya, *Acc. Chem. Res.* **2014**, *47*, 1742–1749; b) M. Endo, H. Sugiyama, *Acc. Chem. Res.* **2014**, *47*, 1645–1653; c) K. Lund, A. J. Manzo, N. Dabby, N. Michelotti, A. Johnson-Buck, J. Nangreave, S. Taylor, R. Pei, M. N. Stojanovic, N. G. Walter, E. Winfree, H. Yan, *Nature* **2010**, *465*, 206–210; d) H. Gu, J. Chao, S. J. Xiao, N. C. Seeman, *Nature* **2010**, *465*, 202–205.

[23] B. Yurke, A. J. Turberfield, A. P. Mills, F. C. Simmel, J. L. Neumann, *Nature* **2000**, *406*, 605–608.

[24] a) C. J. Murphy, A. M. Gole, J. W. Stone, P. N. Sisco, A. M. Alkilany, E. C. Goldsmith, S. C. Baxter, *Acc. Chem. Res.* **2008**, *41*, 1721–1730; b) J. Chao, C. H. Fan, *Sci. China Ser. B* **2015**, *58*, 834; c) X. Lan, Z. Chen, B. J. Liu, B. Ren, J. Henzie, Q. Wang, *Small* **2013**, *9*, 2308–2315.

Received: December 30, 2015
Revised: March 4, 2016
Published online: May 19, 2016

